NINTH EUROPEAN ROTORCRAFT AND POWERED LIFT AIRCRAFT FORUM

Paper No. 14

A COMPARISON WITH THEORY OF PEAK TO PEAK SOUND LEVEL FOR A MODEL HELICOPTER ROTOR GENERATING BLADE SLAP AT LOW TIP SPEEDS

R.R. FONTANA

J.E. HUBBARD, JR.

Department of Mechanical Engineering
Massachusetts Institute of Technology
Cambridge, Massachusetts 02139
U.S.A.

Ninth European Rotorcraft Forum
13-15th Sept. 1983
Stresa, Italy

A COMPARISON WITH THEORY OF PEAK TO PEAK SOUND LEVEL FOR A MODEL HELICOPTER ROTOR GENERATING BLADE SLAP AT LOW TIP SPEEDS

R.R. Fontana
J.E. Hubbard, Jr.

Department of Mechanical Engineering
Massachusetts Institute of Technology
Cambridge, Massachusetts 02139
U.S.A.

ABSTRACT

Mini-tuft and smoke flow visualization techniques have been developed for the investigation of model helicopter rotor blade vortex interaction noise at low tip speeds. These techniques allow the parameters required for calculation of the blade vortex interaction noise using the Widnall/Wolf model to be determined. The measured acoustics are compared with the predicted acoustics for each test condition. Under the conditions tested it is determined that the dominating acoustic pulse results from the interaction of the blade with a vortex 1-1/4 revolutions old at an interaction angle of less than 8°. The Widnall/Wolf model predicts the peak sound pressure level within 3 dB for blade vortex separation distances greater than 1 semichord, but it generally over predicts the peak S.P.L. by over 10 dB for blade vortex separation distances of less than 1/4 semichord.

INTRODUCTION

Helicopter noise is a problem in the use of helicopters for the civilian market. The VTOL capability of helicopters makes them suitable for use in populated areas where space requirements are a primary concern; however, the noise generated by helicopters restricts their usefulness in this environment. The primary source of noise in modern heliocopters is the aerodynamic pressure fluctuations produced by the rotor. The aerodynamic noise generated by the blades can be divided into the two basic groups of broadband noise and harmonic noise. Harmonic noise is related to the blade passage frequency. Blade slap is an impulsive type of noise. These impulses are generally spaced at intervals corresponding to the blade passage frequency. Blade slap is usually the dominant noise source when it occurs.

There are several different flow phenomena which may result in blade slap. At high tip speeds blade thickness effects and unsteady transonic flow may produce impulsive noise. These mechanisms have been studied by Schmitz, Boxwell, Tangler, Farrasatt [1-6] and others. At low tip speeds these effects are not significant and blade slap may be produced solely by fluctuating aerodynamic loading caused by a blade interacting with a vortex trailed from a previous blade. This phenomenon, termed blade vortex interaction noise, has been studied in References [7-10]. Blade vortex interaction noise is the subject of this paper.

Blade vortex interaction noise is most likely to occur under descent conditions when the tip vortices pass close to the rotor disk and during maneuvers in which a tip vortex passes close to a blade, such as in a turn. Hubbard and Leighton have used a scale model to conduct parametric studies of blade vortex interaction noise [11-15]. Cox has done instrumented blade tests on a full scale helicopter using 110 pressure transducers and Hubbard has used instrumented model helicopter blades to study the blade vortex interaction at high angles of attack [16]. Nakamura used the full scale helicopter blade pressure measurements of Cox to determine the acoustic signature due to a blade vortex interaction using a linear theory and concluded that more detailed knowledge of the blade surface pressures was necessary to accurately predict the shape and amplitude of the acoustic pulse [17]. Tangler used a Schlieren flow visualization technique on a high speed model helicopter rotor operating at full scale Mach numbers and found that the blade vortex interaction could produce bow shocks at the speeds tested [3]. Widnall and Wolf [18] have developed a model which predicts that the character of the tip vortex strongly influences the shape and amplitude of the acoustic pulse generated by a blade vortex interaction. Experimental tests by Tangler [19] and Mantay [20] indicate that variations in the tip geometry, which affect the vortex structure, do have a pronounced effect on the amplitude and shape of the blade slap noise pulse. McCormick has investigated the unsteady aerodynamics of helicopters [21], and Farrasat [4] has developed a theory which can predict the sound generated by a rotating blade given detailed information on the blade surface pressures, but this theory is not easily applied until the blade surface pressures can be calculated for a blade vortex interaction or until much more detailed measurements can be made [Nakamura, 17]; the theory of Farrasat is also very complex and requires a considerable amount of computing power.

The theoretical model of Widnall and Wolf [22] predicts the vortex structure, the fluctuating lift produced by the blade interacting with this vortex, and the far-field radiated acoustics due to this fluctuating lift. Thus the theory is very attractive from a designers point of view; however, it includes many assumptions which must be verified before it may be confidently applied to full scale helicopter noise prediction and reduction. The purpose of this research is to determine the validity of some of the most basic assumptions of the Widnall/Wolf model and the feasibility of measurement of some of the required input parameters; then compare the experimentally measured acoustics with the predicted acoustics. Experimental tests used to verify the accuracy of this theory, which does not include shock and other non-linear aerodynamic effects, must be done at low tip Mach numbers so that these effects will not be present in the measured results, and in view of the trend towards higher blade numbers and lower tip speeds such a linearized model might be applied to full scale helicopters without modification for nonlinear effects.

In order to determine the conditions present during blade vortex interaction noise, the validity of the assumptions of the Widnall/Wolf theory, and the input parameters required for the theoretical calculations, two flow visualization techniques for a model helicopter rotor have been developed. To determine the character of the flow over the surface of the blade, a fluorescent mini-tuft technique has been developed. The geometry of the blade vortex interaction has been determined using a smoke flow visualization technique. Tufts are useful for determining the presence of such phenomena as separation and spanwise flow [23-25]. For this work a new technique of mini-tuft photography has been developed which uses existing and relatively inexpensive equipment.

The smoke technique used is a refined version of the technique developed for the M.I.T. Model Helicopter Rotor Acoustics Group by S. Peale et al. [26]. A similar technique of upstream smoke injection has also been used by other researchers [27,28]. The technique developed here allows quantitative measurement of the blade vortex interaction geometry and also provides some new insights into the characteristic vortex structure generated by the model helicopter rotor.

The validity of the most important assumptions of the Widnall/Wolf model is determined and a comparison of the theoretical results with experimental measurements is made.

THEORETICAL MODEL OF WIDNALL AND WOLF

2.1 Description of the Model

The Widnall/Wolf model is an incompressible model which uses inviscid, linear aerodynamic theory and does not include any rotational effects [22]. The theoretical approach is to determine the vortex characteristics then model the blade vortex interaction as a wing flying through a vertical gust to determine the resulting fluctuating lift forces. These lift forces are then assumed to act on the wing surface modeled as a line of acoustic dipoles for the radiated far-field acoustic calculation.

The Betz [29,30] vortex rollup model is used to determine the characteristics of the tip vortex given the spanwise circulation distribution of the blade from the tip to the point of maximum circulation. The Betz model assumes the flow is purely two dimensional and inviscid, and that the rolled up vortex tube is circularly symmetric. Three conservation laws are used to determine the character of the rolled up vortex from the circulation distribution. These laws are that the circulation is conserved, the centroid of vorticity remains at a fixed spanwise location, and the second moment of vorticity is conserved. Assuming that the vorticity trailed from the tip is rolled up into the center of the vortex and the vorticity at each spanwise location is then mapped progressively into an increasing radius of the vortex according to the three conservation laws, the character of the tip vortex may be determined. The important things to note are that the model does not include the effects of rotation, vortex curvature, viscosity, or axial flow, and that the infinite slope at the tip represented by an elliptical circulation distribution results in a line vortex at the center of the rolled up vortex (a finite vorticity concentrated into an infinitesimal area) and is not physically realizable due to viscous effects. An irrotational circulation distribution is assumed to exist outside of the rotational region predicted by the Betz model.

The Betz vortex is then modeled as a vertical upwash on an infinite wing. The vortex is assumed to be a constant distance from the plane containing the path of the airfoil, with the geometry shown in Figure 1a. The vertical components of the vortex velocity field in the plane of the path of the blade are determined and this upwash is modeled as the Fourier integral of its harmonic components. The fluctuating lift due to each harmonic component is calculated using Filotas's linear aerodynamic theory for an infinte span two dimensional wing, and the superposition of these lift fluctuations gives the resulting fluctuating lift produced by the upwash [31]. The Filotas model does not include the effects of compressibility, sweep, rotation, or tip effects, and the modeling of the vortex as harmonic upwash neglects the effects of the chordwise velocity fluctuations and the vortex's self induced movement during the interaction. The most important assumptions of the model of the lift fluctuation are that the flow is incompressible, the vortex motion does not affect the resulting pressures significantly, and the flow remains attached, without separation or stall, during the interaction.

The fluctuating lift calculated from the Filotas theory is then assumed to act on a line of acoustic dipoles on which the lift fluctuation is active over some effective length representative of the length of the blade which interacts with the vortex (Figure 1b). The fluctuations are set to zero outside of this length. The tip effects are modeled acoustically by the abrupt trucation at the ends of this line of dipoles. The assumptions of the acoustic model are: that the wavelength of the radiated sound is much greater than a chord length (compact source assumption), the blade tip effects can be modeled by the instantaneous cut off which is achieved mathematically by a delta function, the velocity and strength of the fluctuating lift are the same all along this dipole line, and there are no rotational effects.

The important assumptions of the Widnall/Wolf model are summarized as follows: 1) The Betz model assumes that the vortex is two dimensional and inviscid. It does not model the rotational effects, and requires knowledge of the circulation distribution. 2) The vortex is assumed to be straight and remain a constant distance from the plane containing the path of the blade at a constant angle λ of Figure 1. 3) The interaction angle must be small so that the pressure fluctuation produced by the interaction of the vortex with the blade is convected at a Mach number greater than one through the surrounding fluid. This condition is met when $\frac{U}{C \sin\lambda}$ is greater than or equal to one; otherwise the tip effects are the primary noise sources and these are not expected to be accurately modeled by the abrupt cutoff condition on a line of dipoles. 4) The motion of the vortex itself and the non vertical components induced by the vortex during the interaction are assumed to have little effect on the lift fluctuations. 5) Knowledge of the blade vortex separation distance and the interaction angle are required input parameters for the fluctuating lift calculation which assumes that the fluid is incompressible and the flow remains attached. 6) The compact source assumption of the dipole model must be met which means most of the acoustic energy must be radiated at wavelengths greater than the blade chord.

For a comparison of experimental results with the theory the important conditions which must be maintained during the experiment are that the geometry of the interaction must be consistant with the geometrical assumptions of the model, and the flow must remain attached during the interaction. Predicted results are very sensitive to the geometrical input parameters of interaction angle and spacing; therefore, these must be accurately determined by the experiment.

It is important to show that the flow remains attached during the blade vortex interaction because there are no currently available simple theoretical methods for dealing with the unsteady aerodynamic loading on wings with separated flow. The model tests have been performed at low Mach numbers to ensure that the incompressible flow assumption of the Filotas model is met and to prevent the intrusion of thickness and transonic flow effects into the measurements. Actual calculation of the predicted acoustics was done using the computer program developed by Wolf. For a detailed discussion of the theoretical model and program see reference [22].

EXPERIMENTAL EQUIPMENT AND TECHNIQUES

3.1 Equipment Description

The model helicopter rotor experiments were done at the M.I.T. 5 x 7 1/2 foot open jet anechoic wind tunnel. During acoustic tests the floor is covered with six inch open cell polyurethane foam. Cremer blocks cover most of the ceiling and wall surfaces. This treatment provides free field conditions down to 160 Hz [32]. The maximum airstream Mach number of this facility is 0.10; therefore, scattering effects due to the shear layer are negligible [33]. Complete documentation on the wind tunnel facilities is available in references [34,35].

The rotor system is driven by a hydraulic motor which is capable of speeds up to 3900 RPM; however, the high speed capabilities of this system were not used for this research since it was desirable to maintain low rotor blade tip Mach numbers to minimize compressibility effects. The maximum rotor speed obtained in these tests was 1000 RPM ($M_{tip} < .3$). Details of the hydraulic motor drive system are available in reference [36].

The model helicopter rotor blades have NACA 0012 airfoil section with 2 inch chord and negative 8° of linear twist from the root to the tip (i.e., 8° washout at the tip). The blades have square tip planforms with balsa tips of revolution on the ends. The blades themselves are mounted on flapping hinges. The collective pitch is manually adjusted for each blade and there is no cyclic pitch or lead lag hinge for the blades. The radius from the center of the rotor hub to the blade tip is 25.6 inches.

The blades are mounted on a hub which is supported by a pair of four spoke flexures to the shaft. These flexures are instrumented with strain gauges to measure the rotor mean thrust. The thrust measurement is conditioned by electronics mounted on the hub and the signals are transferred to the stationary frame through a Lebow slip ring assembly. Further details of the thrust dynamometer are available in references [34,35].

All tests for this research were with zero degree shaft angle (vertical shaft), and the rotor was oriented to thrust downwards (inverted) to reduce the interference of the tunnel floor, and to allow the microphone to be placed directly above the center of the hub (which corresponds to being directly below a helicopter). This orientation is consistent with previous blade slap research in this facility [15]. Acoustic data was taken using a Bruel and Kjaer (B&K) Type 4133, 1/2 condenser microphone in conjuction with a B&K Type 2615 cathode follower. A B&K Type 2604 power supply - amplifier was used to measure the peak and RMS values of the acoustic signal after conditioning by a internal B weighting network. An optical sensor combined with a notched plate mounted under the rotor hub provided a one per revolution pulse which was used for strobe timing purposes. The rotor speed was measured by measuring the period of this signal. A schematic of the instrumentation is given in Figure 2b.

Period and delay time measurements were obtained using a Nicolet 206 Explorer III digital oscilloscope with floppy diskette storage capabilities. This oscilloscope was also used to view and record the acoustic traces.

Tufts are made of polyester fiber 0.0007 inches in diameter which is processed so that it becomes a kinky spiral with a spiral diameter on the order of 0.015 inches. These tufts were died so that they fluoresce visibly under ultra violet radiation for added brightness. The tufts are mounted on 0.5 inch centers on a very smooth glossy black blade with small drops of glue.

Photography of the tufts required careful attention to the camera and strobe positioning. The camera was positioned and focussed then the General Radio 1540 Strobolume stobe was positioned to minimize the light striking the background and glare reflecting from the blade. An Olympus Om-1 35mm camera with power winder and 50mm f1.8 lens was used for the majority of the testing. Ilford HP-5 and XP-1 400 ASA black and white film and Kodak VR-1000 high speed color film produced the best results in the 35mm format. Accurate timing of the strobe was produced by a timer delay circuit which was triggered from the one per rev. signal.

Smoke was generated from a stationary smoke generator consisting of a cylindrical heated tube. The smoke was injected upstream of the rotor and was convected into the rotor disk. Details on the smoke generator are available in Reference [26]. Tuft and smoke experiments could not be done simultaneously or with the same blades because the smoke softened the paint, causing the tufts to stick firmly to the surface. Because the smoke appears grey or white, the best detail is obtained using a black blade. An old tufted blade was used for the smoke photographs, and the tuft orientations visible in the smoke photographs should be ignored since the tufts were stuck to the paint.

EXPERIMENTAL RESULTS AND DISCUSSION

4.1 The Tuft Technique

The tuft technique provides a simple, convenient and inexpensive method for determining the direction of the flow on the surface of the blade. The character of the flow during the interaction is important for determining the applicability of the Widnall/Wolf model. Other parameters related to the flow conditions at azimuth angles between 110° and 170° are also important since they may effect the character of the tip vortex which will later interact with the blade. This technique may also have other applications in the study of helicopter rotor aerodynamics such as the study of retreating blade stall [38].

Tuft response to the flow conditions is shown in Figures 3 and 4. Figure 3a is a single exposure photograph of the suction side of the retreating blade at 225° azimuth and 5° tip pitch. The spanwise orientation of the tufts between 13% span and approximately 75% span show a spanwise flow in this region. Note that some tufts on the leading edge in this region are oriented in a chordwise direction; however, aft of this region the flow appears to be spanwise or even reversed near the trailing edge. From the 75% span to the 92% span position the tuft pattern transitions from a generally spanwise towards the tip orientation to a very orderly chordwise orientation. This indicates a region in which the apparently separated spanwise flow transitions to an attached chordwise flow.

Figure 3b was taken under the same conditions as Figure 3a; however, multiple exposures were used to provide an image which consists of a superposition of several photographs. This provides information about the consistancy of the tuft patterns from revolution to revolution, which in turn indicates the steadiness of the flow. The fanning pattern of the inboard tufts indicate spanwise flow which has a slight variation or unsteadiness. Midspan tufts show a wide fanning pattern which indicates an unsteady "buffetting" type of flow field. The fanning pattern narrows and assumes a chordwise orientation as the tip is approached and the outer 8% of the span shows essentially no fanning of the tufts indicating steady attached chordwise flow in this region.

Observing the tuft behavior at various azimuths indicates that the spanwise flow starts inboard and migrates towards the tip as the blade proceeds into the retreating side of the rotor disk. The spanwise flow region migrates outboard along the span as the 270° azimuth position is approached. By the time the blade reaches the 270° position, the entire span may show strong spanwise flow. As the blade approaches the advancing side chordwise flow appears at the tip and migrates inboard as the advancing side is approached. The azimuth at which these effects begin and end depends upon the tip pitch and advance ratio.

These tests showed that the tufts can indicate the presence of separated spanwise flow and local flow disturbances as well as the presence of attached chordwise flow. The presence of the tufts on the blades did not produce a consistantly measureable change in the characteristics of the blade vortex interaction noise (see Figure 12). Therefore, it is assumed that the disturbance of the tufts does not affect the mechanism which is responsible for blade vortex interaction noise.

Determination of the surface flow conditions present during the blade vortex interaction noise conditions is done by photographing the tufts during the interaction. The distance between the blade and the microphone is measured and the acoustic transmission time is calculated. Using a Nicolet Explorer III digital oscilloscope to measure the acoustics and the flash trigger pulse, while triggering the oscilloscope with a one per revolution signal, the flash trigger timing circuit is adjusted so that the flash occurs before the measured acoustic pulse by an amount equal to the calculated acoustic transmission time. Flash triggering is done over a range of delay times around the time of the interaction because of slight variations in the location of the acoustic pulse and uncertainties in the measurements. The resulting photographs are typical of those shown in Figures 4a and b. There is no apparent change in the flow patterns on the suction side as the blade interacts with the vortex and produces the characteristic acoustic pulse. Note the chordwise orientation of the tufts. In particular, the tip region is very steady. A multiple exposure photograph of the blade spinning with zero tunnel velocity (not hover because of the effects of the tunnel walls and floor) shows the same pattern. It appears that the blade vortex interaction does not produce any visible signs of separated flow and the attached flow assumption of the theory is valid for the conditions tested.

4.2 Description of the Smoke Technique

Smoke was injected upstream of the rotor disk. Because the smoke is already present in the air and is not ejected from the blade itself it does not significantly effect the flow over the blade except for the temperature and density difference of the smoke. The position of any fluid element in the flow field is determined by the time integral of the velocity field acting on that fluid element. In the absence of the rotor wake, smoke upstream is convected downstream and produces a straight horizontal filament of smoke. Velocities produced by the rotor wake will result in distortion of this filament, and the magnitude and direction of the deviation from a straight horizontal filament indicates the effect of this velocity field acting on the smoke over time. Since smoke photographs show the effect of the time integrated velocity field up to the time at which it is observed, smoke is most useful for visualizing flow fields in which isolated effects are present for an adequate time period for the velocity field to move the smoke. Unless the velocity field is essentially steady, the velocity of the flow field must be determined by measuring the velocity of the smoke, and the shape of the patterns will not necessarily reflect the velocity field present at that time.

Figure 5 represents a smoke "movie" in which development of the smoke pattern due to the tip vortex is observed at progressively later stages of its lifetime. The photographs are not actually of the same vortex, but the differences between the smoke images from revolution to revolution are small. The first photograph of Figure 5a shows the blade approaching the smoke which is straight except for the slight deformation by the previous tip vortex located at midspan on the blade. Figure 5b was taken just after the tip of the blade passed through the smoke at 135° azimuth. At this time the vortex has been generated and now crosses through the smoke, but the velocity field has not acted long enough to cause significant displacement of the smoke. Figure 5c shows the effect of the tip vortex on the smoke; a slight "S" shape with a small circular region due to the rapid rotation in the center indicates the presence of the vortex velocity field and its location. In the next photograph the same characteristics as in the previous photograph are present, but the effect of the axial flow in the center of the vortex is more pronounced. This flow has caused the smoke that would be in the center of the vortex to be displaced along the axis of the vortex. This produces the cone shape which has an appearance similar to that of a tornado. The remaining photographs show the history of the vortex and the growth of the scale of influence of the vortex on the smoke as time progresses. Axial flow continues to move the smoke in the center of the vortex along the lengthwise axis of the vortex while the rotational field continues to wrap the smoke around the center and increase the size of the smoke pattern as the velocity field acts over a longer time period. The apparent increase in the size of the smoke pattern does not directly indicate an increase in the vortex size or a change in vortex character.

Figure 5 shows the presence of blade vortex interactions with large interaction angles. These interactions were not responsible for the large blade slap pulses shown in Figure 12. The interaction angle is so large that the trace Mach number of the disturbance through the fluid is not high enough for efficient sound radiation. These large angle interactions were not studied because the acoustic signiture is dominated by the large pulses.

Photographing the smoke just before the interaction with the same technique of delay timing used for the tuft studies, with a camera a location downstream and below the rotor (viewing the suction side), results in the photograph shown in Figure 6. This figure shows the interacting blade just before it is surrounded by the smoke which was distributed along the vortex by the axial flow. In this figure the tunnel flow is from the left to the right. The first vortex which is to the left side of the shaft was just created by the white blade. The second vortex which is just to the right of the shaft was created by the black blade 3/4 of a revolution earlier. The third vortex which produces the blade vortex interaction noise was produced by the white blade 1 1/4 revolutions earlier. Another perspective of the smoke is given (although at a higher advance ratio) in Figure 7. From these photographs it is evident that the the entire span of the blade interacts with the vortex at a small interaction angle. This results in a high velocity (trace Mach number) of the generated pressure fluctuation through the fluid. If this velocity is greater than the sound speed in the fluid then the resulting pressure fluctuation will be radiated efficiently. This is the primary reason that this interaction dominates the acoustic signature.

Photographing the smoke from certain positions allows quantitative measurements of the interaction geometry. Locating the camera directly under the rotor allows the interaction angle to be determined (Figure 8). The measurement itself is accurate to within a few degrees; however, the vortex is curved and the blade rotates as it passes through the vortex, so this angle changes during the interaction. For the theoretical calculations the angle measured just before the blade entered the smoke was used because the angle is most easily measured at this point.

Viewing the interaction from the downstream section of the wind tunnel so that the camera looks directly at the trailing edge of the interacting blade allows the orientation of the vortex with respect to the plane containing the path of the blade to be determined. Figure 9 shows that the vortex is not exactly parallel to the plane of the blade as is assumed by the theory. The skew appears to be on the order of a few degrees. This view also allows the blade vortex separation distance to be determined but shows that this separation distance varies with spanwise location. The variation is on the order of one inch from 1/4 span to the tip.

Another technique for the determination of the blade vortex separation distance is to view the blade tip straight down the span during the interaction as shown in Figure 10. The center of the circular swirling pattern is the center of the vortex at the spanwise location of the smoke stream. Note that the smoke's foggy appearance in the center of the vortex due to mixing and axial flow makes it difficult to determine the blade vortex separation distance accurately. This region can be eliminated by positioning the smoke injector such that the tip passes close to the smoke but does not actually go through it. The resulting motion of the smoke is diagrammed in Figure 13. Since the smoke remains in the essentially inviscid region of the vortex where there is no axial flow, the rotational velocity field forms a wave in the smoke which curls on itself and forms a circle around the vortex. Figure 11 shows the application of this technique in which the center of the vortex can be assumed to lie in the center of the resulting smoke circle, which is well defined since there has been little mixing due to viscous action.

Although accurate determination of the velocity distribution using smoke flow visualization would require several photographs of the same vortex each taken at known short time intervals, estimates of the velocities may be determined from the data included here. The axial flow velocity near the center of the vortex may be estimated by comparing the change in length of the cone shape produced by the axial flow with the time required for this change. This velocity varies with the distance from the center of the vortex and with the age of the vortex, but from Figure 6 it can be estimated that the axial velocity is on the order of 20 to 30% of the tip velocity although by the time the interaction occurs it may be much less. The net circulation of the vortex may be estimated from the rotation of the smoke located in the inviscid region of the vortex. The circulation can be determined by measuring the radius of the circular pattern, the number of rotations the "crest" of the wave has made from its origin, and the time between the start of the vortex induced motion and the photograph. Figure 11 shows the circulation to be on the order of 10 ft^2/second. This corresponds to the advancing blade creating 90% of the mean thrust at this aximuth (150°). Tuft results showed that only the tip of the retreating blade is not dominated by spanwise flow at this time (330° azimuth) which also indicates that the advancing blade is producing most of the thrust at this time.

Smoke allows the geometry of the interaction to be determined, and provides insight on the vortex strength and structure, showing a strong axial flow in the center. This information will be used for the prediction of the noise using the Widnall/Wolf model.

CORRELATION OF RESULTS AND DISCUSSION

5.1 Summary of Parameters

The validity of the use of the theoretical model of Widnall and Wolf to calculate the noise due to the blade vortex interaction depends upon the maintenence of attached flow during the interaction. The presence of attached flow throughout the interaction is verified experimentally under the conditions tested by the tuft technique. Since this basic assumption is correct under these conditions the next step is to determine the geometric parameters of the blade vortex interaction. This is done using the smoke flow visualization technique. Smoke flow studies show that the entire span interacts with the vortex and that blade vortex separation distance and interaction angle vary slightly over the span. The blade velocity also varies linearly with the spanwise position due to blade rotation. The theoretical model does not include the effects of these variations. Because the velocity increases linearly to the tip, it is assumed that only the outer span contributes significantly to the acoustic pressure [37]. For this reason the separation distance and interaction angle were measured near the tip, and the interaction length was assumed to be 25 % of the span (6 inches) for the purpose of the theoretical calculations.

Vortex structure was calculated using a cubic polynomial circulation distribution from the point of maximum circulation to the tip. For these calculations it was assumed that 90% of the measured mean thrust was being generated by the vortex producing blade at 150° azimuth. The maximum value of the circulation was calculated assuming a linear circulation distribution from the root to the point of maximum circulation located at 75% span, and a cubic polynomial circulation distribution from the point of maximum circulation to the tip. The lift produced by this distribution in terms of the maximum circulation was determined including the effect of rotation and free stream velocity. The value of the maximum circulation is determined using 90% of the measured thrust value for the lift. Details of the circulation and lift distribution used are given in Appendix 1 of Reference 40.

Comparison of measured and calculated acoustics is done on a point by point basis because it is not convenient to hold one parameter, such as blade-vortex interaction angle, fixed since varying the advance ratio varies the thrust, interaction angle, and separation distance. Holding the advance ratio fixed maintains approximately constant blade vortex interaction angle, but varying the blade pitch to change the thrust will also vary the blade vortex separation distance. These tests were done by maintaining a fixed rotor shaft speed and tip pitch and varying the tunnel speed to change the advance ratio.

The first three conditions shown in Table 1 correspond to three different advance ratios with the blade pitch and rotational speed held constant at 5° (tip) and 800 RPM. The B weighted peak sound pressure becomes a maximum and is dominated by the blade slap pulse (for the microphone location directly above the inverted rotor) at an advance ratio of .17 under these conditions. When the advance ratio is increased or decreased from this 'peak' slap value, the blade slap signal decreases and the azimuthal location at which the interaction occurs changes. At the 'peak' slap condition, Figures 9 and 10 show the tip of the blade passing very close to the center of the vortex with the vortex located about 0.25 inches below the suction side of the blade near the tip. It is also clear from Figure 9 that the blade-vortex spacing is much larger inboard. This orientation occurs because the tip path plane is tilted in a descent mode under these conditions. Figure 8 shows the blade and the vortex to be essentially parallel (0° interaction angle) during this peak slap interaction. This results in a rapid variation in pressure over the span (a high trace mach number).

Using the measured values summarized in Table 1 and the stated assumptions, the peak sound level predicted by the Widnall/Wolf theory is 109 dB while the measured peak sound level (B weighted) is 97 dB. The effect of variations in each input parameter on the theorectically predicted peak sound pressure for this case is given in Figure 14. Figure 14a shows the effect of thrust on the predicted peak sound level. Increasing the thrust increases the circulation of the vortex. The increased velocity in the vortex results in a larger amplitude of the pressure fluctuation and a greater predicted peak sound level. Figure 14b illustrates the effect of blade vortex separation distance on the peak sound level. Decreasing the separation distance increases the peak velocity of the upwash and decreases duration of the interaction. The higher frequency and amplitude caused by reduction in the blade vortex spacing results in a strong influence of blade-vortex spacing on the predicted peak sound level. The effect of the interaction angle on the predicted peak sound level is given in Figure 14c. Increasing the interaction angle lowers the velocity of the pressure fluctuation through the fluid (the effective or trace Mach number) and lowers the frequency of the pressure fluctuation on the blade. These effects result in a lower predicted peak sound level with an increase in the interaction angle. The small increase in the predicted peak sound pressure from the interaction angle of $\lambda = 0°$ to a maximum at $\lambda = 2°$ appears to be contrary to the expected behavior and the reason for this behavior is not clear at this time, but may be due to computational errors. The effective interaction length effects the peak sound pressure as shown in Figure 14d. As the interaction length is increased from zero, the predicted peak sound level increases rapidly then plateaus to a very gradual slope.

The theoretically predicted peak sound level of 109 is over 12 dB higher than the measured value of 97 dB and Figures 14a through 14d show the measurement errors could not be responsible for this large a discrepancy. Further insight into the differences may be gained by comparison of the measured and predicted pulse shapes shown in Figures 15a and 15b respectively. The time between the peak (maximum and minimum) values for the predicted pulse is on the order of 0.3 milliseconds whereas for the measured acoustic pulse this time is on the order of 0.9 milliseconds. This indicates that the pressure fluctuation is actually more spread out than is predicted by the theory, and suggests that the vortex may have a broader character than that predicted by the Betz model. This could be caused by the fact that the actual vortex has a strong axial flow and is 1 1/4 revolutions old before the interaction occurs. The Betz vortex does not account for axial flow or viscous effects, and viscous effects may be important because of the age of the vortex. The smoke convected along the vortex by axial flow always appears diffuse (foggy) by the time the interaction occurs, and the fact that the smoke has become mixed or diffuse indicates that viscous effects may have become important. Another factor not accounted for by the model is the effect of the large angle interactions (shown in Figure 5), which preceed the small angle interaction responsible for blade slap under these conditions, on the vortex structure. The assumption of a linear-cubic polynomial circulation distribution for the Betz calculation may also be incorrect; a more gradual load tapering would spread the predicted vortex velocity distribution. In any case a spread velocity distribution would result in a reduction of the high frequency content of the fluctuating lift, and this would result in a reduction of the peak to peak amplitude of the predicted acoustic pulse.

Further insight may be gained by noting that the predicted acoustic pulse (Figure 15b) has a small positive excursion followed by large negative excursion. The measured acoustic pulse shows the opposite trend with a large positive excursion followed by a small negative excursion. While the peak to peak amplitude is determined by the behavior between the peaks, the larger size of the positive peak indicates that the initial positive fluctuation is more rapid and/or of greater amplitude than predicted, this could be caused by the inaccuracy of the upwash model or the fluctuating lift model which is dependent on the upwash model. The peak to peak amplitude of the acoustics is dominated by the character and amplitude of the region between the maximum upwash and downwash velocities. The pulse is much more spread for the experimentally measured case than the predicted case, and this is most likely to be due to the inaccuracy of the model near the center of the vortex.

When the advance ratio is reduced from the "peak" blade slap value of 0.17 to 0.15, the tip path plane and vortex spacing changes and the interaction noise occurs at a larger azimuth (54°). The blade vortex interaction geometry may again be determined from the smoke flow visualization. The interaction angle is increased to about 6°. The center of the vortex is about 0.25 inches above the pressure side of the blade near the tip, while the center of the vortex is on the suction side on the inner span. The predicted blade slap acoustic pulse is 100 dB (peak), and the measured acoustic pulse is 90 dB peak (B Weighted). The predicted and measured acoustic pulse shapes show the same characteristics as for the "peak" blade slap case of μ = .17. The predicted pulse shows a time of 0.38 milliseconds between the maximum and minimum values and the measured pulse shows again essentially three times the predicted value with 1.2 milliseconds between the peak values. Because the blade-vortex separation distance is the same as for the "peak" slap case, and the only parameters which have changed are the interaction angle and the thrust of the vortex producing blade, the trends for variations in the input parameters are similar to the "peak" blade slap case. As for the "peak" blade slap case, the inaccuracy of the theory is caused by the close proximity of the center of the vortex with the blade.

Increasing the advance ratio above the "peak" blade slap condition of 0.17 to 0.19 changes the tip path plane and vortex spacing. The blade slap producing interaction occurs earlier at an azimuth of ~40°. Smoke flow visualization again allows the important parameters of the interaction geometry to be determined. The interaction angle is 4 degrees for this case. The entire vortex lies below the blade, and Figure 11 shows that near the blade tip the blade vortex separation distance is 1.7 inches and the interaction appears to occur in a region where the flow remains essentially inviscid. The predicted blade slap acoustic pulse is 87 dB and the measured peak value is 90 dB (B weighted). Figures 16a and b show the variation in the predicted peak sound level λ and I.L. are varied. In this case the predicted value is close enough to the measured value that a reasonable change in a parameter could put the predicted value above or below the measured value. For example, assuming an effective interaction length of 9 inches instead of 6 inches results in a predicted value equal to the measured value. The pulse shapes for the measured and predicted acoustic pressure are given in Figures 17a and 17b respectively. In this case the predicted acoustic pulse has a time between peaks of 1.4 milliseconds and the measured pulse has a time between peaks of ~.9 milliseconds. This is a reversal of the trend shown for the previous two cases and the difference between the values is not as great as for the previous cases. It is also interesting to note that the pulse shape of the measured acoustic pressure no longer has the large positive pressure peak and now has a slightly greater negative than positive excursion, although this is still not as much so as with the theoretically predicted pulse shape. The theoretical model of Widnall and Wolf appears to perform much better for a large blade vortex separation distance when the structure of the vortex is not as important. At this separation distance the blade passes through the essentially irrotational part of the vortex and the only significant vortex related parameter here is the net circulation.

Table 1 also gives the measured parameters and the theoretically predicted and measured peak sound level for several other operating conditions. The trend is the same as for the previously discussed cases - the theory over-predicts the peak pressures when the blade vortex separation distance is small, and is reasonably accurate when the blade vortex separation distance is large.

Using the parameters determined from the smoke flow visualization and making the stated assumptions allows the noise due to the blade vortex interaction to be calculated using the Widnall/Wolf theory. Theoretically predicted values agree well with the measured values for the high advance ratio (above peak slap) conditions when the blade-vortex separation is large. Under these conditions, the blade interacts with the essentailly irrotational region of the vortex flow and the character of the vortex as predicted by the Betz model is not important. When the blade vortex spacing is small the theory over predicts the peak sound level. This could be caused by inaccuracies in the Betz model, inacurracy in the assumed circulation distribution, inaccuracies in the modeling of the vortex as an upwash, inacurracy in the Filotas lift transfer function, or a combination of these effects.

CONCLUSIONS AND RECOMMENDATIONS

Two flow visualization techniques have been developed for model helicopter rotor flow visualization studies. These techniques have been used to investigate the blade vortex interaction noise model of Widnall and Wolf by determining the validity of some of the critical assumptions of the theory and comparing the predicted results with those measured in the experiments.

The fluorescent mini-tuft technique allows the characteristics of the flow over the surface of the blade to be determined. Experiments with the tufts indicated that there is no separation or stall on the suction side during the blade vortex interaction under the tested conditions. This shows that fluctuating lift models used for noise prediction models need not include the effects of separated flow. The theoretical model uses the linear theory of Filotas which assumes attached incompressible flow. The blade tip Mach number in these experiments did not exceed 0.3 and the tufts indicated that there was no separation during the interaction, so the attached flow assumption of the Filotas model was essentially met under the tested conditions. The tufts also indicated strong spanwise flow on the retreating side and may be useful for the study of such phenomena [38].

The smoke technique shows that the blade vortex interaction responsible for blade slap under these conditions occurs when the trailed tip vortex interacts with the entire span of the blade at a small interaction angle. This condition is a requirement for the use of the Widnall/Wolf model; however, it also introduced the effect of rotation which is not accounted for in the model. This makes it difficult to determine an effective interaction length since the entire span of the blade interacts with the vortex, but the velocity varies over the entire span. The contribution of the inboard span is small compared with that of the tip, however, the transition is gradual and any assumed interaction length is somewhat arbitrary. A modification of the theory which could eliminate the problem of determining an effective interaction length is presented in Appendix 2 of reference [40]. The smoke flow visualization studies also indicated that the blade vortex separation distance and interaction angle vary over the span. The variation in the blade vortex spacing has the greatest effect on the predicted peak acoustic pressure. The proposed modification outlined in Appendix 2 may also be useful in correcting for these effects. An instrumented blade which provides information on the spanwise variation of the fluctuating load during the interaction could be effectively used in conjunction with this modification [16].

The smoke flow visualization technique allows the critical parameters of blade vortex separation distance and interaction angle to be determined and these measurements allowed the theoretically predicted acoustic pressure to be calculated for direct comparison with the measured acoustic pressure for various operating conditions. These calculations showed that the theory predicts a peak acoustic pressure which is close to the measured value at test conditions for which the center of the vortex did not pass close to the blade (large blade vortex separation distance), but over predicted the peak acoustic pressure when the center of the vortex passed close to the blade (small separation distance). Large blade vortex separation reduces the effects of both vortex structure and self induced vortex motion which is not modeled by a vertical upwash. At small spacings the vortex structure becomes important, and the modeling of the vortex as an upwash spectrum may no longer be valid. The smoke technique indicates axial flow in the vortex, and shows that viscous effects may be important since the vortex is 1 1/4 revolutions old by the time the interaction occurs. The Betz model does not account for either of these effects. A pressure instrumented blade could be used to determine the blade loading so that the accuracy of the blade circulation assumption could be determined, and a more accurate circulation distribution could be used if enough pressure transducer locations are present along the span. Information on the behavior of the vortex during the interactions with the blades and the motion of the vortices in the rotor wake could be studied by using the smoke technique with high speed movies. By analyzing the motion of the smoke with digital computer techniques and digitized images of the photographs, the velocities may be determined. The viability of the digitizing process has been shown using some of the photographs included in this report. The measurement of the velocity distribution in the vortex would allow the actual vortex structure to be used for the calculation of the upwash spectrum and this would allow the accuracy of the upwash approximation and fluctuating lift model to be determined.

If this upwash approximation is correct then the extension of the theory for compressibility effects may be warranted. Martinez [39] has developed a closed form solution for the near and far field pressure due to a finite span airfoil interacting with a vertical upwash including compressibility effects, and this theory could be substituted for the fluctuating lift and far field pressure calculations for high Mach numbers ($M > .7$). The ability to substitute and improve the Widnall/Wolf theory in sections, and the relative simplicity of each part of the theory are strong points for its use in the prediction of blade vortex interaction noise.

A direct analogy of the results of these model tests with full scale helicopters cannot be made without some consideration of the large difference in scales. In particular, the vortex structure may be very dependent upon the blade boundary layer thickness and character. The maximum Reynolds numbers of these model tests is 0.2×10^6 based on the chord while full scale Reynolds numbers are typically fifty times higher at $\sim 10 \times 10^6$. The relatively thinner boundary layer of the full scale blade would be expected to result in a less significant axial flow component.

In summary the tuft studies showed attached flow on the suction side during the blade vortex interaction responsible for blade slap under these conditions. The tufts may also be useful for the study of retreating blade stall or other aerodynamic events which might cause separation. The smoke flow visualization experiments provided the information on the geometry of the blade vortex interaction and allowed the theoretical model of Widnall and Wolf to be used for the prediction of the peak far field pressure due to the blade vortex interaction. The accuracy of the theory for large blade vortex spacings and the over prediction of the theory for small blade vortex spacing suggests that the vortex structure is not accurately predicted by the theory, or, the blade vortex interaction may not be accurately modeled by the upwash and fluctuating lift models. Experimental determination of the vortex structure and motion during the interaction may allow the significance of each of these effects to be evaluated. In particular the determination of the vortex structure could be used to determine the accuracy of an improved vortex model, the accuracy of the upwash model, and the effect of various blade modifications on the vortex structure.

ACKNOWLEDGEMENTS

The authors would like to express their gratitude for the support and advice of Professor Wesley L. Harris throughout this research effort. This work was sponsored in part by NASA Langley Research Center under Grant NSG 1583 and NASA Ames Research Grant NAG 182.

REFERENCES

1. F.H. Schmitz and D.A. Boxwell: In-Flight Far Field Measurement of Helicopter Impulsive Noise. Journal of the American Helicopter Society, Vol. 21, No. 4, October 1976.

2. F.H. Schmitz and Y.H. Yu: Theoretical Modeling of High Speed Helicopter Impulsive Noise. Presented at the Third European Rotorcraft and Powered

Lift Aircraft Forum, Aix-en-Provence, France, Sept. 7-9, 1977 (Paper No. 54).

3. J.L. Tangler: Schlieren and Noise Studies of Rotors in Forward Flight. Presented at the Thirty-third Annual National Forum of the American Helicopter Society, Washington, D.C., May 1977.

4. F. Farassat: Theory of Noise Generation from Moving Bodies with an Application to Helicopter Rotors. NASA Technical Report, TR R-451, Langley Research Center, December 1975.

5. C.R. Vause, F.H. Schmitz, and D.A. Boxwell: High Speed Helicopter Impulsive Noise. Preprint No. 1004, presented at the Thirty-second Annual National Forum of the American Helicopter Society, May 1976.

6. W.E. Bausch, C.L. Munch, and R.G. Schlegel: An Experimental Study of Helicopter Rotor Impulsive Noise. USAAVLABS Technical Report 70-72, June 1971.

7. J.E. Hubbard, Jr. and W.L. Harris: Measured Surface Pressure and Velocity Trends on a Highly Loaded Model Helicopter Rotor Experiencing Blade Slap. Fluid Dynamics Research Lab Report 81-6, MIT, Cambridge, Massachusetts, October 1981.

8. S. Chu: Helicopter Noise Due to Blade/Vortex Interaction. Master's Thesis, MIT, Department of Aeronautics & Astronautics, June 1971.

9. S. Widnall, S. Chu, and A. Lee: Theoretical and Experimental Studies of Helicopter Noise due to Blade-Vortex Interaction. Presented at the Helicopter Noise Symposium, Durham, North Carolina, September 1971.

10. S.E. Widnall: Helicopter Noise Due to Blade-Vortex Interaction. Journal of the Acoustical Society of America, Vol. 50, No. 1, Part 2, 1971.

11. J.E. Hubbard, Jr. and K.P. Leighton: A Comparison of Model Helicopter Rotor Primary and Secondary Blade/Vortex Interaction Blade Slap. Presented at the 8th AIAA Aeroacoustics Conference, Atlanta, Georgia, April 11-13, 1983.

12. J.E. Hubbard, Jr. and K.P. Leighton: Some Results of a Preliminary Investigation of Model Helicopter Rotor Secondary Blade Slap. Presented at the National Technical Association Region II Student Symposium, Hampton, Virginia, March 1980.

13. J.E. Hubbard, Jr., N.G. Humbad, P. Bauer, and W.L. Harris: Parametric Studies of Model Helicopter Blade Slap and Rotational Noise. MIT Fluid Dynamics Research Laboratory Report No. 79-1, Cambridge, MA, February 1979.

14. J.E. Hubbard, Jr. and W.L. Harris: An Investigation of Model Helicopter Rotor Blade Slap at Low Tip Speeds. Presented at the AIAA Fifth Aeroacoustics Conference, Seattle, WA, March 1979.

15. J.E. Hubbard, Jr.: A Parametric Study of Model Helicopter Blade Slap. Master's Thesis, MIT, Department of Mechanical Engineering, 1978.

16. C.R. Cox: Helicopter Rotor Aerodynamic and Aeroacoustic Environments. Presented at the AIAA Fourth Aeroacoustics Conference, Atlanta, Georgia, October 1977.

17. Y. Nakamura: Prediction of Blade-Vortex Interaction Noise from Measured Blade Pressure. Presented at the Seventh European Rotorcraft and Powered Lift Forum, Garmisch-Partenkirchen, Federal Republic of Germany, September 1981 (Paper No. 32).

18. S.E. Widnall and T.L. Wolf: Effect of Tip Vortex Structure on Helicopter Noise due to Blade-Vortex Interaction. Journal of Aircraft, Vol. 17, No. 10, p. 705, October 1980.

19. J.L. Tangler: The Design and Testing of a Tip to Reduce Blade Slap. Presented at the Thirty-first Annual National Forum of the American Helicopter Society, Washington, D.C., May 1975 (Preprint 963).

20. W.R. Mantay, P.A. Shidler, and R.L. Campbell: Some Results of the Testing of a Full-Scale Ogee Tip Helicopter Rotor; Acoustics Loads, and Performance. AIAA Paper 77-1340, October 1977.

21. B.W. McCormick: Studies Relating to Steady and Unsteady Aerodynamics of Helicopters. Presented at the Helicopter Noise Symposium, Durham, North Carolina, September 1971.

22. T.L. Wolf: The Effect of Tip Vortex Structure on Helicopter Noise due to Blade/Vortex Interaction. Master's Thesis, MIT, Department of Aeronautics & Astronautics, June 1978.

23. J.P. Crowder: Add Fluorescent Minitufts to the Aerodynamic's Bag of Tricks. Astronautics and Aeronautics, Vol. 16, No. 11, p. 54, November 1980.

24. J.P. Crowder: Fluorescent Mini-Tufts for Non-Intrusive Flow Visualization. McDonnel Douglas Corporation, MDC J7374, February 1977.

25. J. McMasters and B. Lamson: The Flight Research Institute. Journal of the Soaring Society of America, Vol. 46, No. 7, July 1982.

26. K.P. Leighton, J.F. Hubbard, Jr., S. Peale, and W. Harris: Parametric Studies and Flow Visualization of Model Helicopter Rotor Blade Slap. Presented at the Seventh AIAA Aeroacoustics Conference, Palo Alto, California, October 1981 (Preprint No. 81-2002).

27. Army Researchers Utilize Smoke Signals for Rotor Design. Vertiflite, Vol. 29, No. 4, p. 53, May/June 1983.

28. R.H. Schlinker and R.K. Amiet: Tail Rotor Blade-Vortex Interaction Noise. Presented at the 8th AIAA Aeroacoustics Conference, Atlanta, Georgia, April 11-13. 1983.

29. A. Betz: Behavior of Vortex Systems. NACA TM 713, 1932.

30. V. Rossow: On the Inviscid Polled-Up Structure of Lift Generated Vortices. Journal of Aircraft, Nov. 1973.

31. L.T. Filotas: Theory of Airfoil Response in a Gusty Atmosphere - Part I, Aerodynamic Transfer Function. UTIAS Report No. 139, University of Toronto, October 1969.

32. K.P. Leighton: A Parametric Study of Model Helicopter Rotor Blade Slap at Moderate Tip Speeds. Master's Thesis, MIT, Department of Aeronautics & Astronautics, February 1981.

33. R.K. Amiet: Correction of Open-Jet Wind Tunnel Measurements for Shear Layer Refraction. AIAA Paper No. 75-532, March 1975.

34. S.E. Widnall, W.L. Harris, A. Lee, and H.M. Drees: The Development of Experimental Techniques for the Study of Helicopter Rotor Noise. NASA CR-137684, 1974.

35. W.L. Harris and A. Lee: The Development of Experimental Techniques for the Study of Helicopter Rotor Noise. Presented at the AIAA Second Aeroacoustics Conference, March 1975.

36. K.P. Leighton: Determination of a Mach Number Scaling Law for Model Helicpoter Rotor Blade Slap. Engineer's Thesis, MIT, Department of Aeronautics & Astronautics, September 1983.

37. N.G. Humbad and W.L. Harris: On the Acoustic Power Emitted by Helicopter Rotor Blades at Low Tip Speeds. Journal of Sound and Vibration, Vol. 66, No. 2, p. 290, 1979.

38. W.J. McCroskey and S.L. Pucci: Viscous-Inviscid Interaction on Oscillating Airfoils. Presented at the AIAA Nineteenth Aerospace Sciences Meeting, St. Louis, Missouri, January 1981.

39. R. Martinez and S.E. Widnall: Unified Aerodynamic-Acoustic Theory for a Thin Rectangular Wing Encountering a Gust. AIAA Journal, Vol. 18, No. 6, p. 636, [Article No. 80-4055].

40. R.R. Fontana: A Determination of Flow Field Characteristics Responsible for Model Helicopter Rotor Blade Vortex Interaction Noise and a Comparison with Theory. Master's Thesis, MIT, Department of Mechanical Engineering, September 1983.

TABLE 1

Blades: NACA 0012 two inch chord -8° linear twist (washout)
Rotor Radius: 25.6 inches
Microphone location during experiment: 52.25 inches above the hub (inverted rotor)
Corresponding microphone position for theoretical calculations -
R = 56.8 inches θ = 247° Ψ = 90°
Interaction length (I.L.) = 6 inches for predicted peak SPL calculations

Measured Parameters							Predicted Peak SPL*
Tip Pitch (degrees)	Ω (RPM)	μ	90% Thrust (lbf)	λ (°)	h/c (semichord = 1")	Peak SPL (B-weighted)*	
5	800	.17	4.9	0	0.25	97	109
5	800	.15	4.7	6	0.25	90	100
5	800	.19	5.1	4	1.70	90	87
5	1000	.17	7.6	0	0.25	105	113
5	1000	.15	7.4	6	0.25	90	101
8	800	.18	5.7	0	0.85	98	98
8	800	.16	5.5	4	0.00	89	115
8	800	.21	5.8	6	2.10	89	85
8	1000	.18	8.9	0	0.85	104	103
8	1000	.16	8.6	4	0.00	96	120
8	1000	.21	9.1	6	1.40	96	95

* Db re. 20 μ Pascal

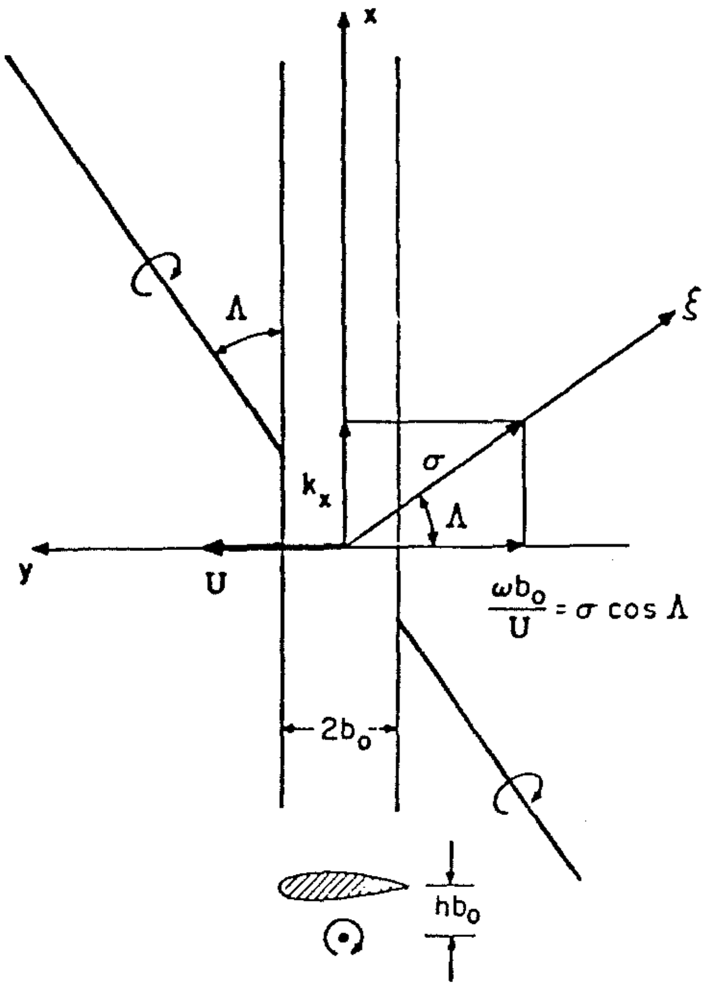

Figure 1a) Geometry of Blade/Vortex Interaction (from Reference 22)
(Note: $c \cong b_o$ (the blade semichord) for this paper)

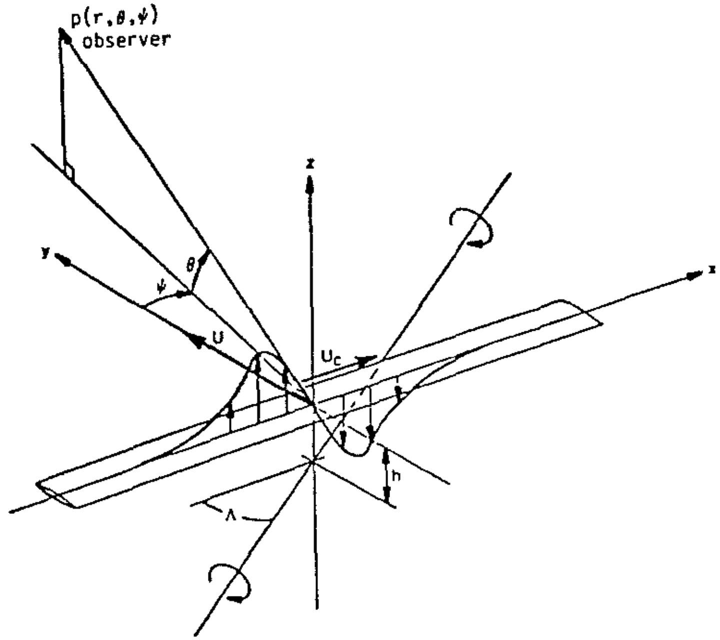

Figure 1b) Geometry of Acoustic Model (form Reference 22)

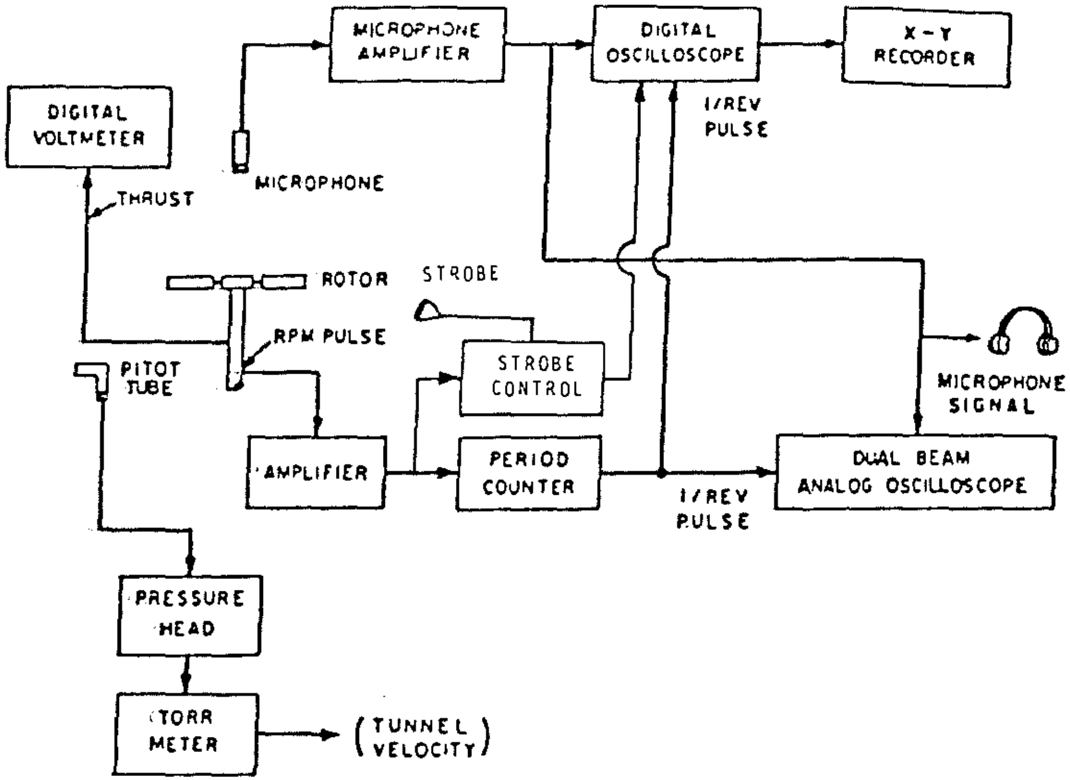

Figure 2. Schematic of Instrumentation used in Data Acquisition

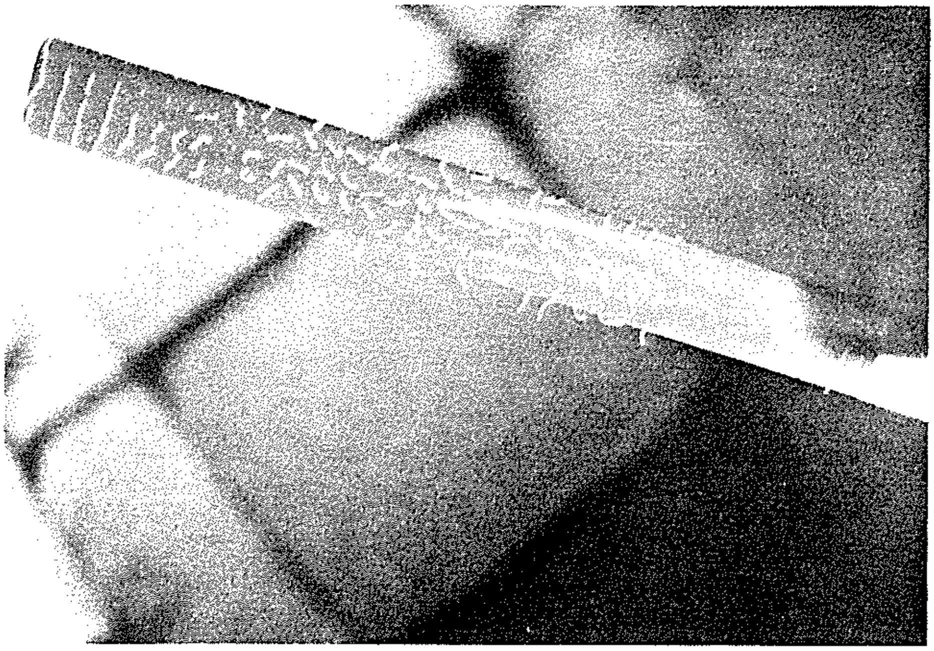

a) Single exposure showing spanwise flow

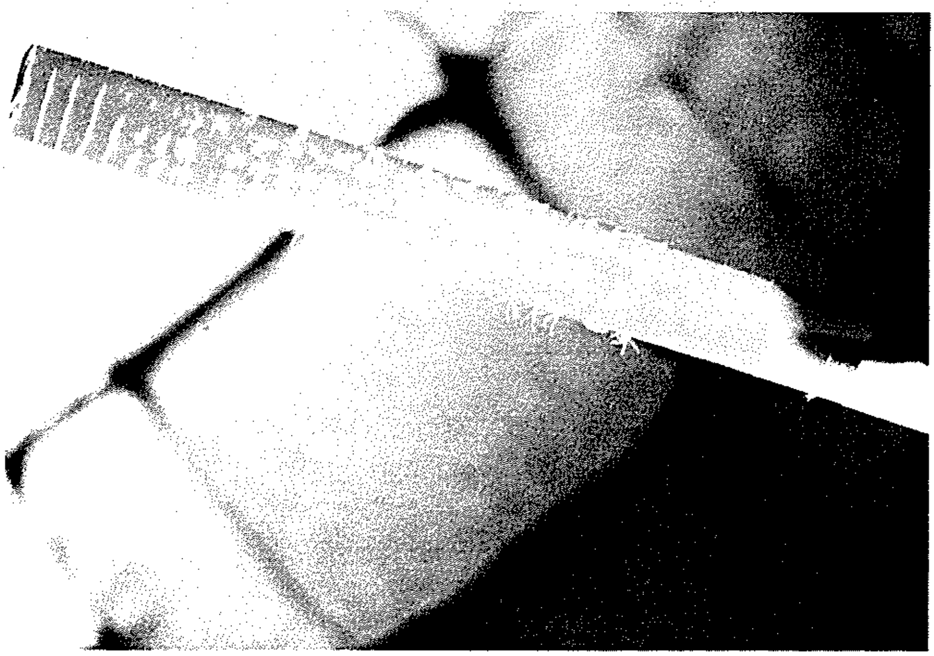

b) Multiple exposure showing the character of spanwise flow

Figure 3. Tuft flow visualization of retreating blade at 210° azimuth
$\mu = .17$ $\Omega = 800$ RPM $\Theta_{TIP} = 5°$

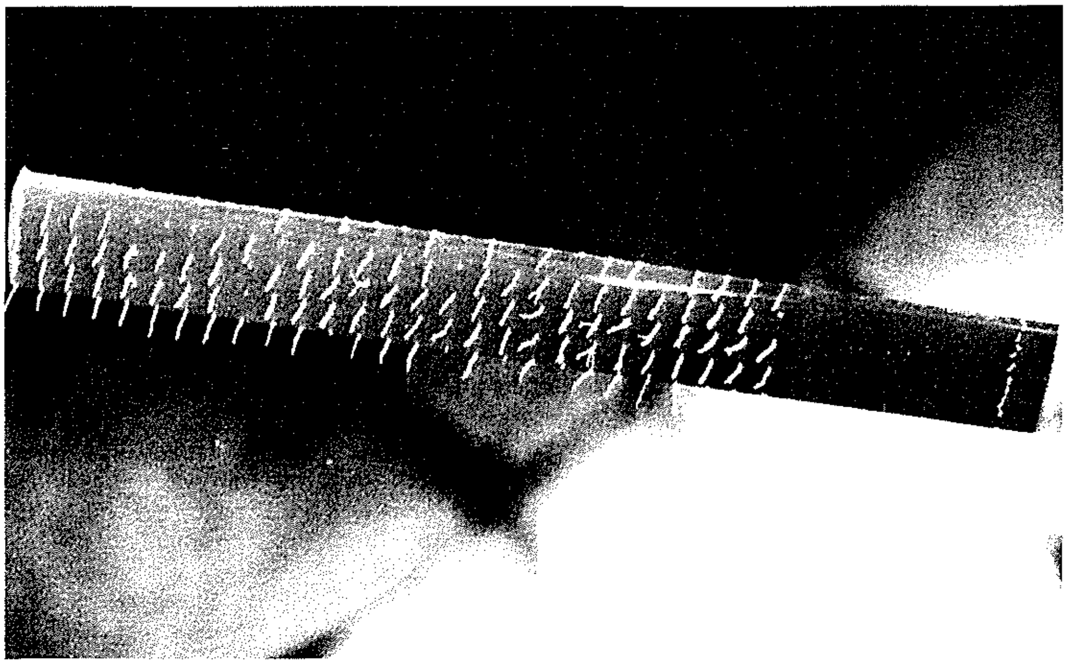

a) Single exposure during blade vortex interaction

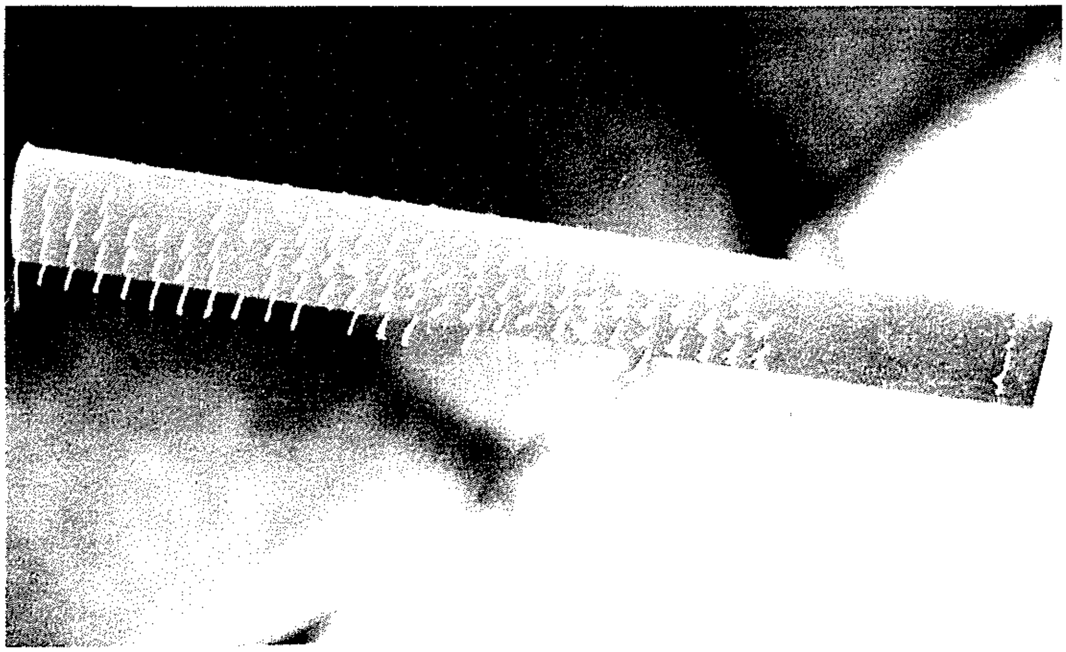

b) Mutiple exposure showing the character of the tuft behavior during blade vortex interaction

Figure 4. Tuft behavior during the blade vortex interaction at 45° azimuth
$\mu = .17$ $\Omega = 800\,RPM$ $\psi \sim 45°$ $\Theta_{TIP} = 5°$
Measured peak sound level 98 Db

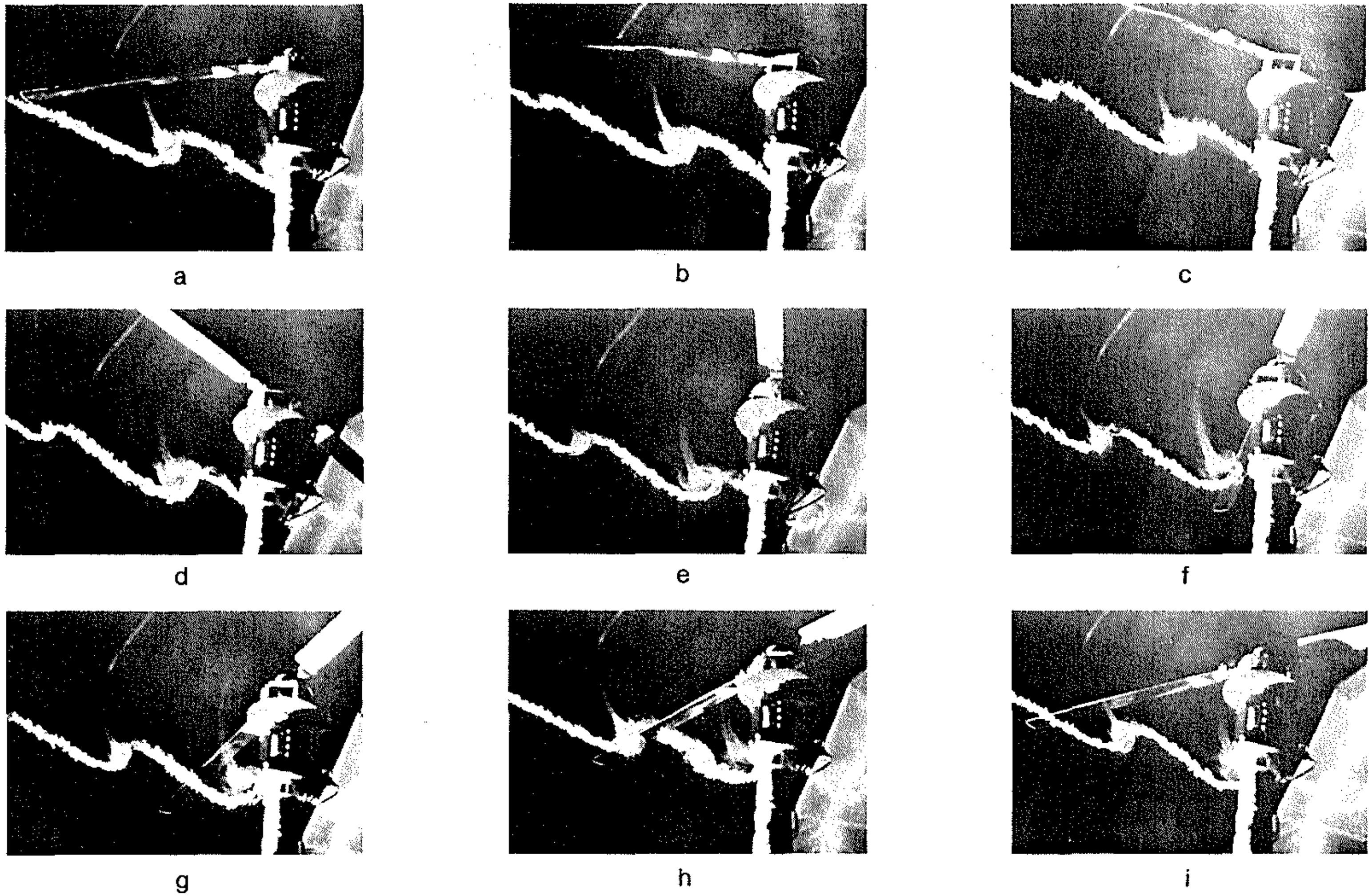

Figure 5. Development of the smoke pattern due to the action of the tip vortices

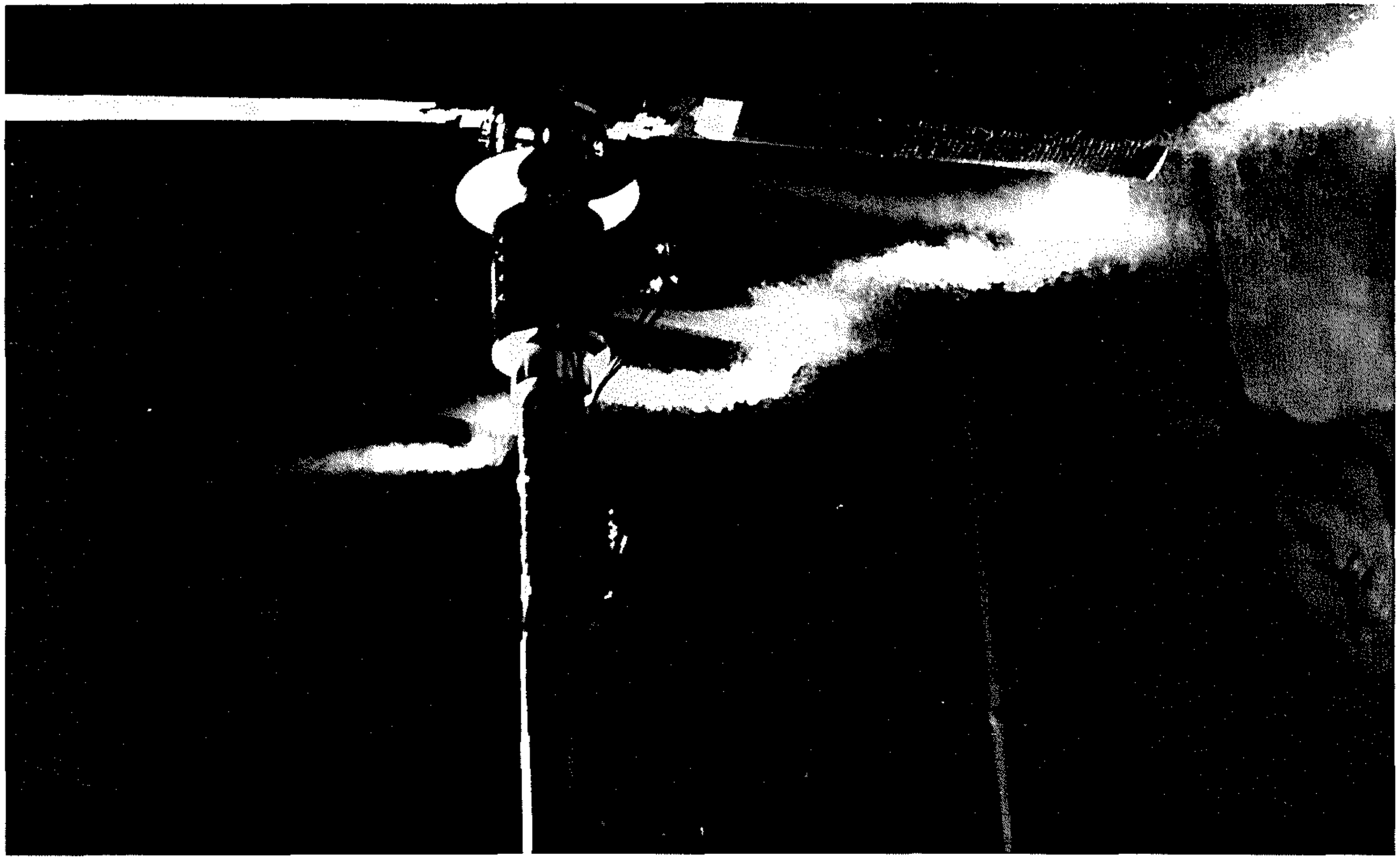

Figure 6. Photograph of the smoke flow visualization taken just before the blade vortex interaction responsible for blade slap $\mu = .17$ $\Omega = 800$ RPM $\psi_{B.V.I.} = 45°$ $\Theta_T = 5°$

Figure 7. View from 30° azimuth of the smoke flow visualization during the blade slap producing interaction under "off peak" conditions
$\mu = .19$ $\Omega = 800$ RPM $\psi \sim 40°$ $\Theta_{TIP} = 5°$

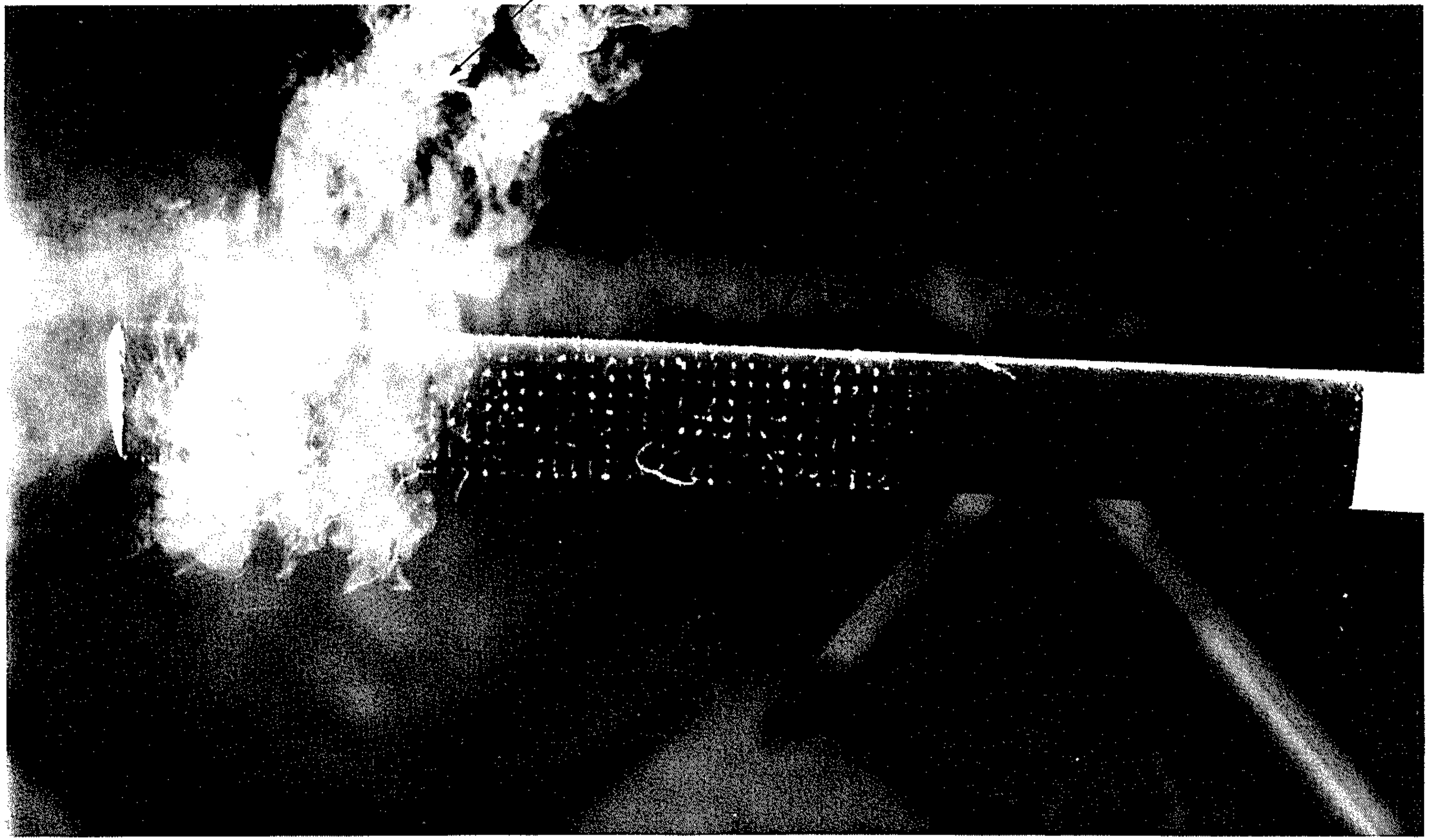

Figure 8. Smoke flow visualization showing the blade-vortex interaction angle during "peak blade slap" conditions $\mu = .17$ $\Omega = 800$ RPM $\psi = 45°$ $\Theta_{TIP} = 5°$
Measured interaction angle $\lambda \sim 0°$

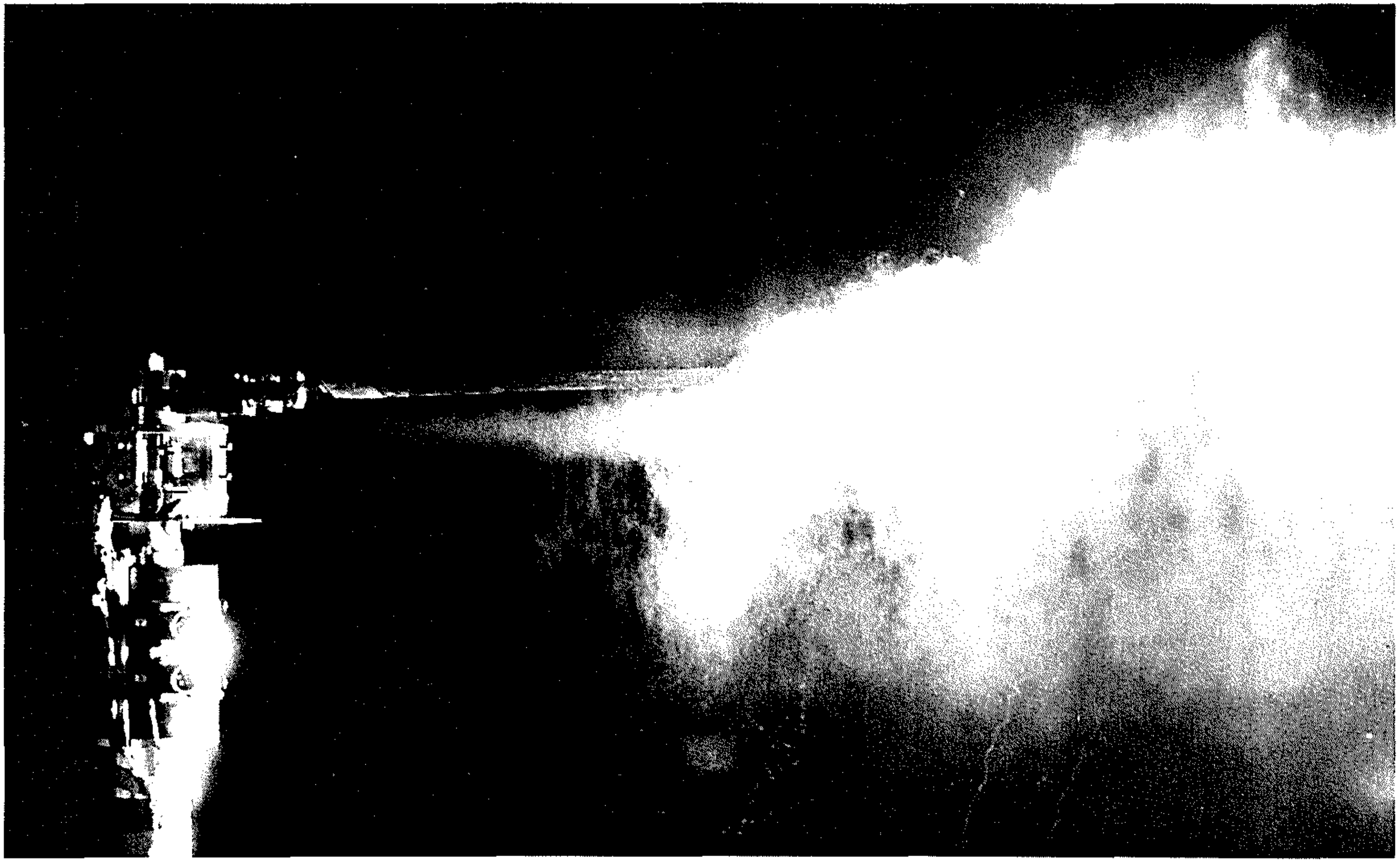

Figure 9. Orientation of vortex along the span during "peak blade slap" conditions
$\mu = .17$ $\Omega = 800$ RPM $\psi \sim 45°$ $\Theta_T = 5°$

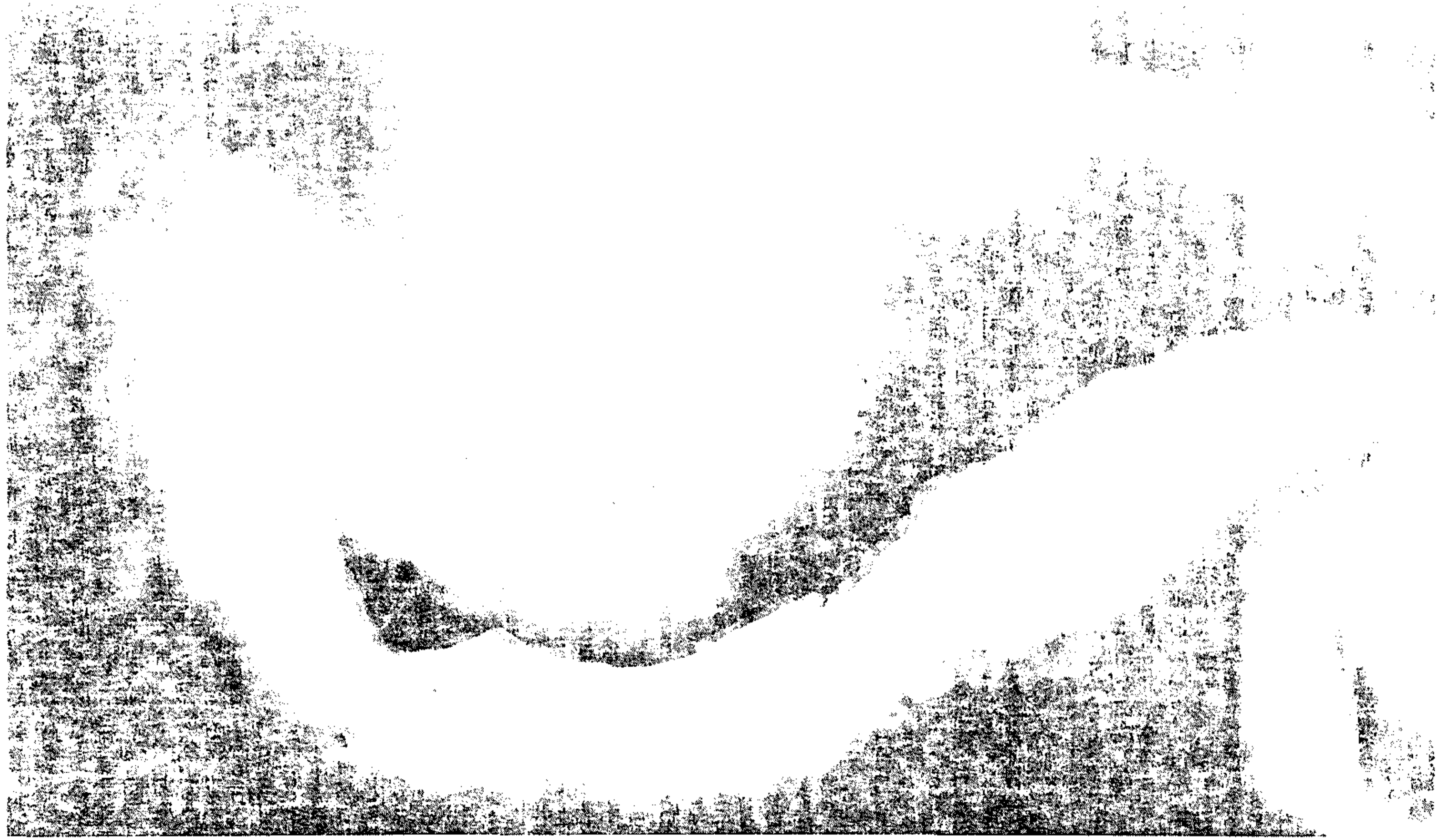

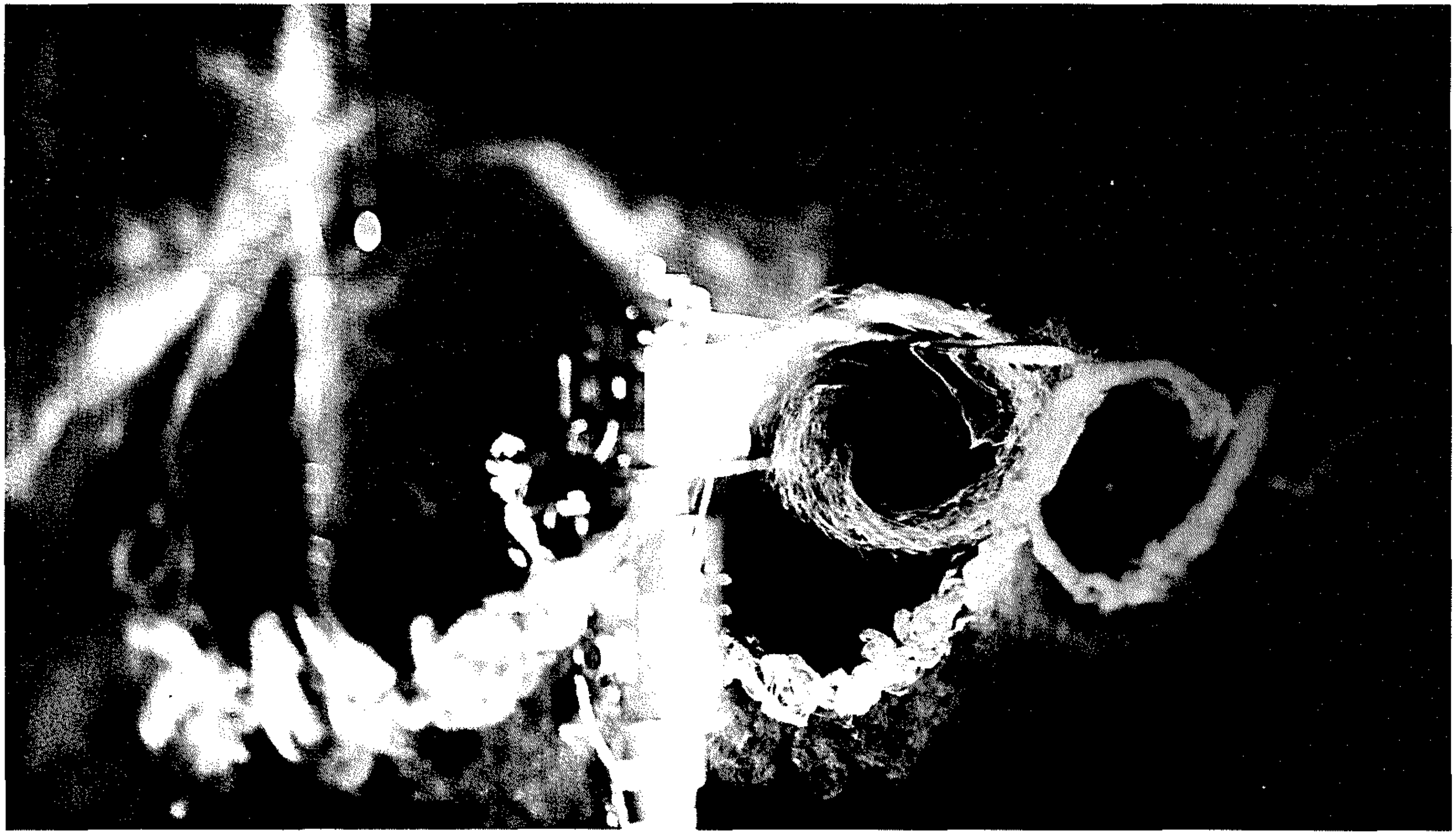

Figure 11. Smoke flow visualization of the blade vortex interaction resulting in blade slap during "off peak" conditions
$\mu = .19$ $\Omega = 800$ RPM $\psi \sim 40°$ $\theta_T = 5°$
Measured blade vortex separation distance ~ 1.7 inches

WITHOUT TUFTS μ=.17 8ØØRPM T.P.=5DEG.

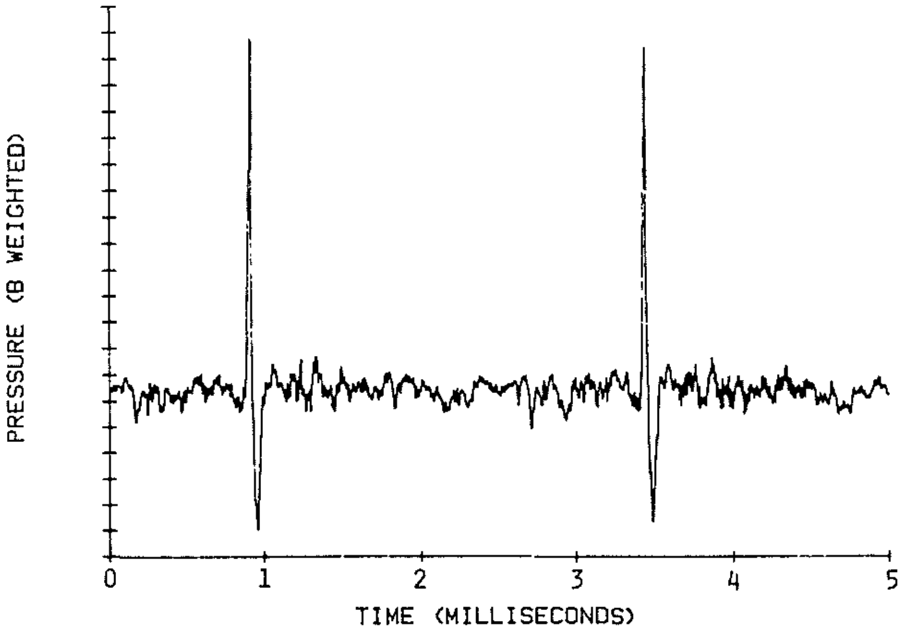

WITH TUFTS μ=.17 8ØØRPM T.P.=5DEG.

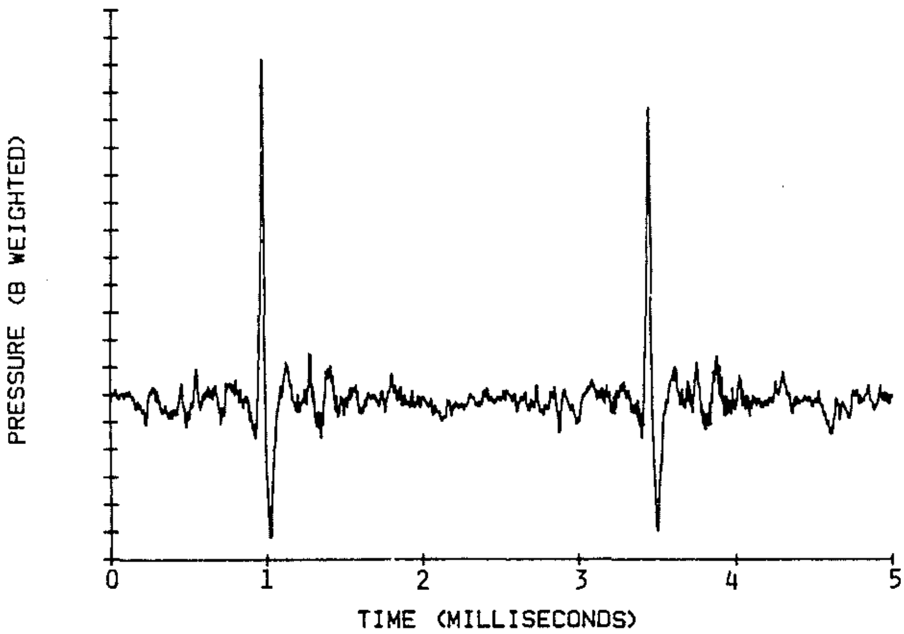

Figure 12. Comparison of Acoustic Trace with and without the Tufts

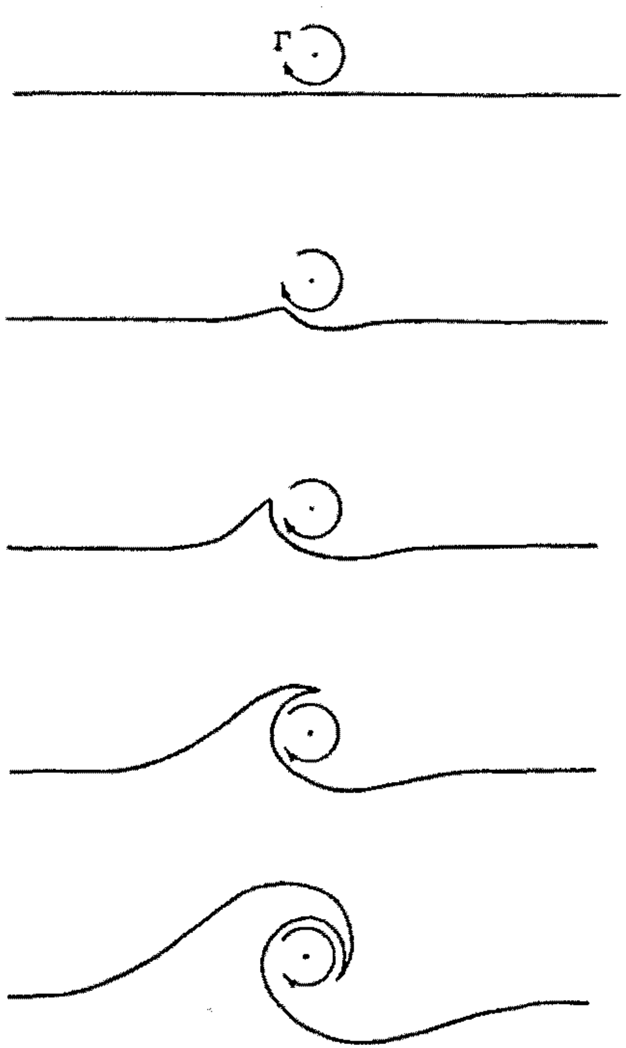

Figure 13. Development of Smoke Pattern with Smoke in Essentially Inviscid Region of Vortex

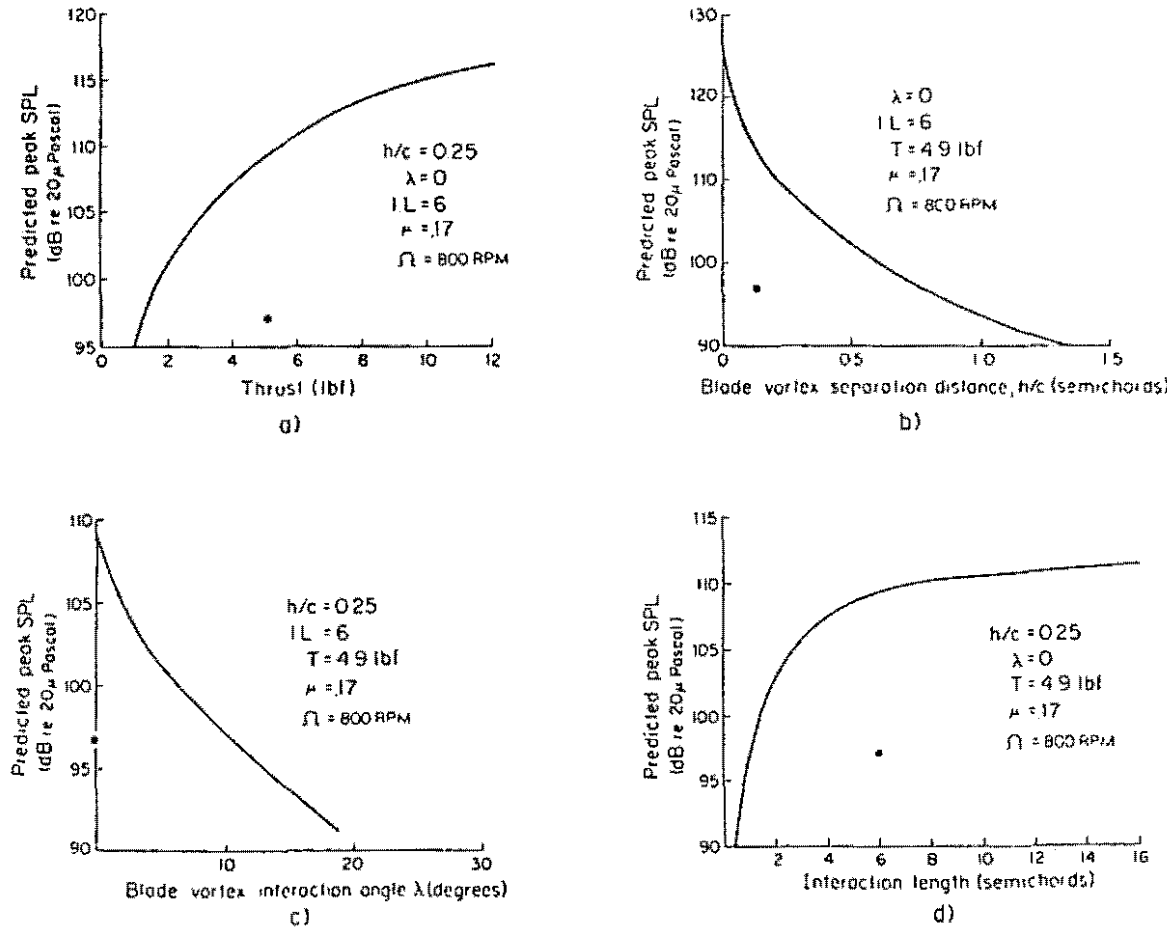

Figure 14. Effect of Variations in Input Parameters on the Predicted S.P.L.

* Measured Value

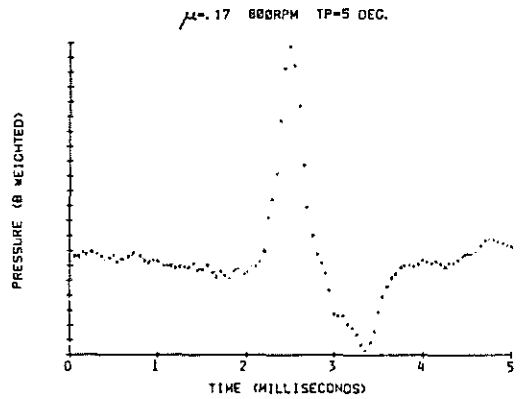

Figure 15 a) Measured Pulse Shape μ=.17 (Peak S.P.L. 97 dB)

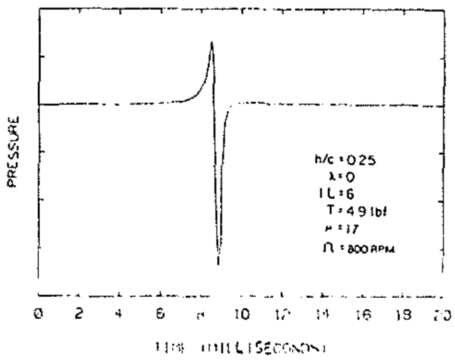

Figure 15 b) Predicted Pulse Shape μ=.17 (Peak S.P.L. 109 dB)

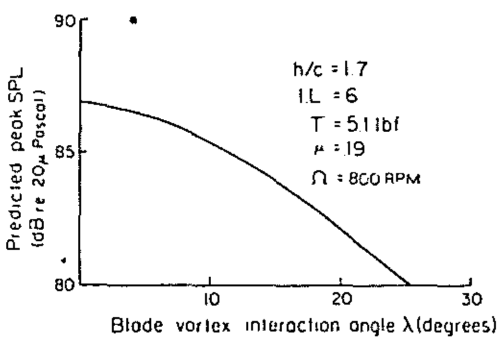

a)

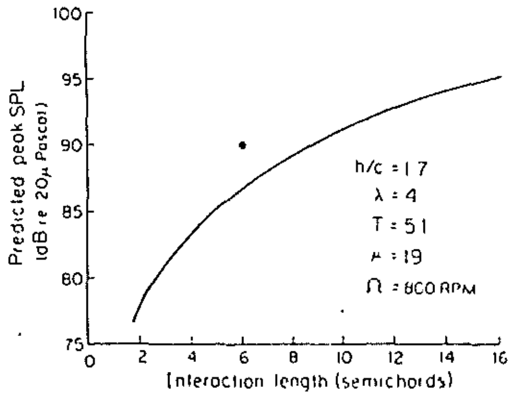

b)

Figure 16. Effect of Variations in Input Parameters on the Predicted S.P.L. for Large Blade Vortex Separation Distance

* Measured Value

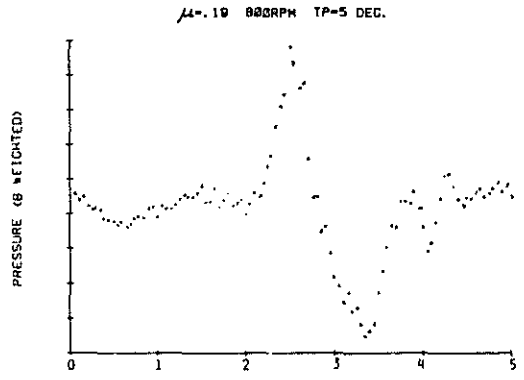

Figure 17 a) Measured Pulse Shape μ=.19 (Peak S.P.L. 90 dB)

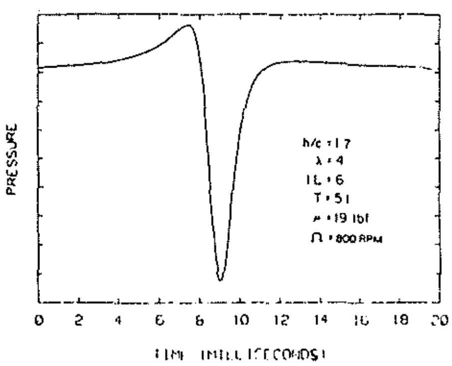

Figure 17 b) Predicted Pulse Shape μ=.19 (Peak S.P.L. 87 dB)